Electrical and photoelectrical characterization of undoped and S-doped nanocrystalline diamond films

Cite as: J. Appl. Phys. **103**, 084905 (2008); https://doi.org/10.1063/1.2908884
Submitted: 08 October 2007 • Accepted: 06 March 2008 • Published Online: 24 April 2008

P. Kulkarni, L. M. Porter, F. A. M. Koeck, et al.

Electrical and photoelectrical characterization of undoped and S-doped nanocrystalline diamond films

P. Kulkarni,[1] L. M. Porter,[1,a)] F. A. M. Koeck,[2] Y.-J. Tang,[2] and R. J. Nemanich[2]
[1]*Department of Materials Science and Engineering, Carnegie Mellon University, Pittsburgh, Pennsylvania 15232, USA*
[2]*Department of Physics, North Carolina State University, Raleigh, North Carolina 27695, USA*

(Received 8 October 2007; accepted 6 March 2008; published online 24 April 2008)

Nanocrystalline diamond (NCD) films are being intensively researched for a variety of potential applications, such as optical windows, electrochemical electrodes, and electron emitting surfaces for field emission displays. In this study Zr, Ti, Cu, and Pt on intrinsic and lightly sulfur-doped (*n*-type) NCD films were electrically and photoelectrically characterized. Intrinsic and sulfur-doped NCD films were synthesized on 1 in. diameter quartz and silicon substrates by microwave plasma assisted chemical vapor deposition. All metals showed linear (Ohmic) current-voltage characteristics in the as-deposited state. The Schottky barrier heights (Φ_B) at the metal-film interface were investigated using x-ray and ultraviolet photoelectron spectroscopies. The undoped NCD films exhibited a negative electron affinity and a band gap of 5.0 ± 0.4 eV. The Φ_B were calculated based on this band gap measurement and the consistent indication from Hall measurements that the films are *n*-type. The Φ_B values were calculated from shifts in the core-level (C1*s*) peaks immediately obtained before and after *in situ*, successive metal depositions. The Φ_B values for Zr, Ti, and Pt on undoped films were calculated to be 3.3, 3.2, and 3.7 eV, respectively. The S-doped films also showed increasing Φ_B with metal work functions: 3.0, 3.1, and 3.4 eV for Zr, Ti, and Pt, respectively. In general accordance with the barrier height trends, the specific contact resistivity (ρ_c) values increased with the metal work functions for both undoped and S-doped films. For the undoped films ρ_c increased from 3×10^{-5} Ω cm^2 for Zr to 6.4×10^{-3} Ω cm^2 for Pt. The ρ_c values for the S-doped films were approximately two orders of magnitude lower than those for the undoped films: 3.5×10^{-7}–4.5×10^{-5} Ω cm^2 for Zr and Pt, respectively. The Hall-effect measurements indicated that the average sheet resistivity and carrier concentration values were 0.16 and 3.5×10^{18} cm^{-3} for the undoped films and 0.15 Ω cm and 4.9×10^{19} cm^{-3} for the S-doped films. © *2008 American Institute of Physics*. [DOI: 10.1063/1.2908884]

I. INTRODUCTION

Diamond and diamond-based thin films, such as diamondlike carbon, and polycrystalline and nanocrystalline diamond, have been used in hard coatings, surface acoustic wave sensors,[1] field-effect transistors,[2] optical windows,[3] bioimplantable electronics,[4] conformal coatings for microelectromechanical systems,[5] high-power and high-frequency devices,[6] and electron emitting surfaces in field emission displays.[7] The chemical inertness, toughness, surface smoothness, range of electrical conductivities, and relative ease of fabrication of certain carbon-based materials make them especially attractive for such applications.

The hydrogen-terminated diamond surface has been identified as a promising cold cathode material because of its negative electron affinity (NEA).[8,9] The presence of a NEA means that the conduction band minimum lies above the vacuum level. Thus, any electrons in the conduction band can transit into vacuum without surmounting a surface barrier. However, a stable supply of electrons to the surface is necessary for steady field emission. This criterion explains the need for *n*-type diamond films.

There has been considerable research regarding the synthesis of *n*-type diamond; impurities such as sulfur, phosphorus, and nitrogen have been investigated as potential *n*-type dopants. Nitrogen is a common impurity in diamond films. It is a deep-level donor impurity with an activation energy of 1.7 eV;[10] this large activation energy makes the homoepitaxial, or polycrystalline, diamond films insulating at room temperature.

However, in NCD films, nitrogen is preferentially incorporated into the grain boundaries rather than the grains and increases electronic states associated with sp^2-bonded carbon atoms residing at the grain boundaries. Incorporation of nitrogen leads to an upward shift of the Fermi level, thereby increasing the electrical conductivity possibly by hopping and impurity band conduction.[11]

Phosphorus-doped homoepitaxial diamond (111) films grown using PH_3 as the dopant gas were also found by *n*-type.[12] The Hall mobility increased with temperature and a maximum mobility of 23 cm^2/V s was reported. The temperature dependence of mobility and its low value suggest that charge transport is mediated through the crystal imperfections.[13]

Theoretical results indicate that sulfur is the most promising *n*-type dopant, with an activation energy of 0.375 eV.[14,15] While there is a significant disagreement on

a)Electronic mail: lporter@andrew.cmu.edu.

the doping efficacy of sulfur in diamond,[16] there have been some experimental results on homoepitaxial diamond that support the theoretical results and suggest that shallow donor levels (0.38 eV) are associated with the incorporation of sulfur; a mobility of 597 $cm^2/V\,s$ was measured using the Hall effect.[17,18]

Recent scanning tunneling microscopy and scanning tunneling spectroscopy studies on NCD films showed the undoped NCD films to be weakly *p*-type (Fermi level slightly below midgap) and the sulfur-doped NCD films to be *n*-type (Fermi level above midgap).[19] It was suggested that a donor state is associated with S, and thus *n*-type doping would be expected with increasing sulfur concentration. Direct evidence of sulfur acting as a donor impurity (in the classical doping sense) is still lacking and is a subject of investigation.[20]

The morphology of the NCD film has been described as a composite of grains containing tetrahedrally sp^3-bonded carbon atoms and grain boundaries containing predominantly trigonally sp^2-bonded carbon atoms.[21,22] Nanometer-size grains influence the mechanical and chemical properties such as hardness, surface roughness, and chemical inertness; whereas the sp^2-bonded grain boundaries, defects, and impurities largely determine the electrical and optical properties, such as the electronic density of states (DOS) and the conductivity of the NCD film.[23] By carefully engineering the morphology, such as the grain size and the sp^2/sp^3 ratio, of poly- and nanocrystalline diamond, it is possible to have some control over the electronic and mechanical properties.

The electronic DOS of NCD comprises two types of states: σ-σ^* states associated with σ-bonds of sp^2 and sp^3 domains and π-π^* states associated with π-bonds in the sp^2, and possibly sp^1, domains. The σ-σ^* states are separated by a band gap of $\sim$5 eV, while the filled π and empty π^* states lie closer to the Fermi level and mainly lie within the σ-σ^* band gap. Hence the π-π^* states play an important role in the optical and electronic properties of NCD. The size, concentration, and orientation of the sp^2 domains also strongly contribute to the electronic structure.[24,25]

Frequency dependent conductivity measurements have shown that the carrier transport through these films is controlled by the grain boundaries. At low voltages, Ohmic transport has been correlated to the presence of sp^2-bonded grain boundaries as evidenced by hopping transport at low temperatures.[26]

Certain factors that impede the use of diamond grown by chemical vapor deposition (CVD) in electronic applications include the lack of *n*-type doping, the high cost of diamond substrates, and the high surface roughness and high stress of diamond thin films. The NCD films offer solutions to the aforementioned limitations. Additionally, materials integration of diamond for electronic applications requires reliable Ohmic contacts with low contact resistances that can be fabricated at low temperatures.

In this study, we have fabricated room temperature, low contact resistance Ohmic contacts to undoped and S-doped NCD films using four metals that span a considerable range of work functions. Also, room temperature Hall-effect measurements were carried out to assess the film type. We have photoelectrically characterized the contacts using x-ray photoelectron spectroscopy (XPS) and ultraviolet photoelectron spectroscopy (UPS) to evaluate the Schottky barriers at the metal-film interfaces.

II. EXPERIMENTAL

Electronic-grade quartz and low-resistivity ($<1\ \Omega$ cm) Si $\langle 100 \rangle$ substrates with diameters of 25 mm were used as substrates for the growth of NCD films. Prior to the deposition of the films, the substrates were ultrasonicated for 30 min in a titanium/diamond/ethanol suspension to seed the growth of nanocrystalline diamond. The substrates were then inserted into a 1500 W AsTeX IPX3750 microwave-plasma assisted CVD chamber and exposed to the plasma for 80 min.

The process gases were "zero-grade" CH_4, H_2, and H_2S (for the S-doped films only). The chamber pressure was maintained at 20 Torr during the film growth. For undoped NCD films, the flow rates were 180 SCCM (SCCM denotes standard cubic centimeters per minute) H_2 and 20 SCCM CH_4. Flow ratios for growing S-doped NCD films were $H_2S+H_2:H_2:CH_4$: 10:170:20 SCCM. The concentration of H_2S in the gas stream was 50 ppm. The substrate temperature and microwave power were maintained at 900 °C and 900 W, respectively. The films were 200 nm thick as measured by *in situ* laser reflectance interferometer.

A Philips XL-30 scanning electron microscope (SEM) was used to characterize the surface morphology of the films prior to metal deposition. Low magnification ($<100\times$) SEM images were used to confirm the dimensions of the patterned metal layers.

For electrical measurements, samples were grown on quartz substrates in order to avoid electrical effects from the substrate. Zr, Ti, Cu, and Pt films of 1000 Å thickness were evaporated at room temperature from elemental sources (source purity >99.9%) and deposited on different areas of the samples using a 3 kW electron-beam evaporation gun in a ultrahigh vacuum (UHV) chamber at pressures $<2\times10^{-8}$ Torr. Circular transfer length method (CTLM) patterns on undoped and S-doped films were fabricated using conventional photolithography. Ohmic contacts were characterized by current-voltage (*I-V*) measurements for the calculation of specific contact resistance (ρ_c). The *I-V* measurements were collected using an HP 4155B semiconductor parameter analyzer that was connected to a Signatone® S-1060H-4QR prober. Two-probe *I-V* measurements were conducted on "as-deposited" samples for all metals. The measurements were performed in a dark room, at room temperature, and atmospheric pressure. Electrical contact to the CTLM pattern was made by placing one probe on the inner circle and one probe on the field (outside the annular ring) contact (Fig. 1). After measuring the *I-V* characteristics, the metal layers were etched, and the same samples were used for Hall-effect measurements. Hall-effect measurements were performed to determine the majority carrier type, concentration, and mobility using a 7500/9500 Lakeshore® Hall-effect measurement system. For these measurements, patterned Ti and Zr contacts on undoped and S-doped NCD

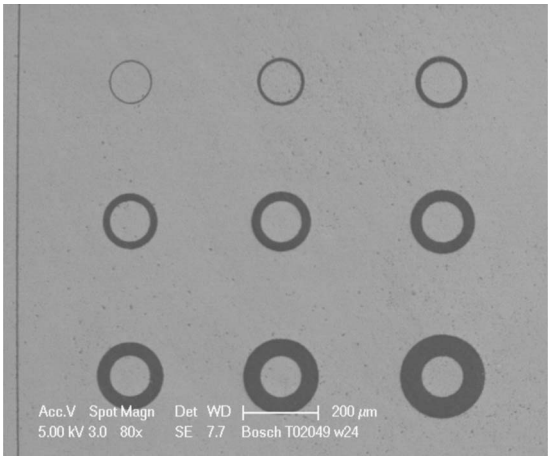

FIG. 1. SEM image of patterned metal layer on undoped NCD film on quartz.

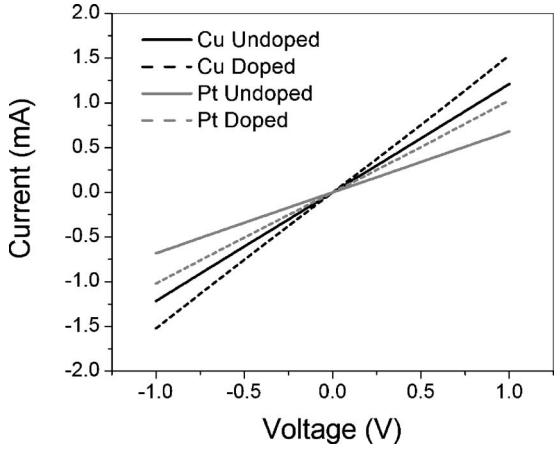

FIG. 2. *I-V* characteristics of Cu and Pt contacts to undoped and S-doped NCD films at 95 μm spacing.

films grown on quartz substrates were etched using 50% HNO_3 solution in water. The etched areas on both samples were then cut into 7×7 mm^2 squares using a precision vertical diamond wire saw. Thin metal wires were connected in the van der Pauw pattern and Hall parameters were recorded at room temperature.

To obviate the problem of film charging, NCD films grown on low resistivity Si substrates were used for the XPS and UPS studies. All *in situ* cleaning and characterizations were conducted in a unique UHV configuration that integrated several analysis and surface processing chambers via a transfer line having a base pressure of 1×10^{-9} Torr. The samples were heated in UHV ($<5.0\times10^{-10}$ Torr) at 800 °C for 20 min to remove hydrocarbons and oxygen from the surface. The samples were then exposed to a remotely excited (600 W microwave electron cyclotron resonance) H_2 plasma at 20 mTorr for 2 min. *In situ* XPS surveys and UPS spectra of the "bare film" were then collected. The samples were then transferred in vacuum to an electron-beam evaporation chamber where ultrahigh purity (>99.9%) Zr, Ti, and Pt were evaporated on different samples. After every 5 Å of metal deposition, the samples were then moved to the XPS chamber and then the UPS chamber for analysis. This process was continued until the total thickness of the metal films was 15 Å.

All XPS spectra were acquired using a Mg $K\alpha$ source ($h\nu$=1253.6 eV) operated at 13 kV and 20 mA emission current in tandem with a hemispherical electron energy analyzer VG CLAM II with a mean radius of 100 mm. Periodic scans of the Au $4f_{7/2}$ peak of a gold foil were used to calibrate binding energies. After each metal deposition, a survey scan and high resolution scans for metal (Zr3d/Ti2p/Pt4f), carbon (C1s), and oxygen (O1s) were collected.

The UPS system consisted of an Omicron® HIS 13 vacuum ultraviolet discharge lamp powered by a NG HIS power supply. The system emits He I radiation at 21.2 eV at a base pressure of 5×10^{-10} Torr; it is used in conjunction with a 50 mm radius hemispherical electron energy analyzer (VSW HA 50). The samples were biased 2–3 V to overcome the work function of the analyzer.

III. RESULTS AND DISCUSSION

A. Electrical characterization

Figure 1 shows a SEM image of a patterned metal layer on an undoped NCD film on quartz. The radius of the inner circle is 50 μm and the radii of the outer rings are 55, 60, 65, 70, 75, 80, 85, 95, and 105 μm from top left to bottom right. All contacts to either the undoped or S-doped films were Ohmic in the as-deposited state. Figure 2 shows the *I-V* characteristics of Cu and Pt contacts on undoped and S-doped NCD films; for clarity, the results for the other contacts are not shown here.

The specific contact resistance (ρ_c, in Ω cm^2) and the contact resistance (R_c, in Ω) were calculated from a linear relationship between the total resistance and spacing between the contacts.[27,28] The CTLM used in this study was proposed by Marlow and Das.[29] It consists of a circular metal contact separated from a (Ohmic) field by an annular gap (Fig. 1). According to this method, a constant current is applied between the inner circle and the field contact, which results in a voltage drop across the metal contacts and the semiconductor layer in between them. The resistance R between the CTLM contacts is given by[30]

$$R=\frac{R_{\mathrm{sh}}}{2\pi}\left[\ln\left(\frac{R_2}{R_2-s}\right)+L_T\left(\frac{1}{R_2-s}+\frac{1}{R_2}\right)\right], \tag{1}$$

where R_{sh} is the sheet resistance of the semiconductor, R_2 is the radius of the outer annular ring, s is the spacing between the circular contact and the field contact ($R_2=R_1+s$), and L_T is the transfer length. The transfer length is a measure of the effective contact length (i.e., the length over which most of the current is transferred) and is dependent on the sheet resistance of the semiconductor and the specific contact resistance. The logarithm term can be expanded as a Taylor series, and Eq. (1) can be rewritten as[31]

$$R=\frac{R_{\mathrm{sh}}}{2\pi R_1}[s+2L_T]c, \tag{2}$$

where c is the correction term given by

TABLE I. Sheet resistance (R_{sh}) and specific contact resistance (ρ_c) values for undoped and S-doped NCD films.

	Work function (eV)	Undoped films		S-doped films	
		R_{sh} (Ω cm)	ρ_c (Ω cm^2)	R_{sh} (Ω cm)	ρ_c (Ω cm^2)
Zr	4.05	1.2×10^{-1}	3.0×10^{-5}	1.1×10^{-1}	3.5×10^{-7}
Ti	4.33	1.6×10^{-1}	1.4×10^{-4}	1.1×10^{-1}	1.3×10^{-5}
Cu	4.65	1.6×10^{-1}	3.8×10^{-4}	1.3×10^{-1}	2.1×10^{-5}
Pt	5.65	2.1×10^{-1}	6.4×10^{-3}	1.9×10^{-1}	4.5×10^{-5}

$$c = \frac{R_1}{s}\ln\left[\frac{R_2}{R_1}\right]. \tag{3}$$

The correction factors can be calculated for the spacings shown in Fig. 1.

Plots of the corrected resistances versus spacings for all of the contacts to undoped and S-doped NCD films showed linear behavior. For the calculation of contact resistance, it was assumed that the sheet resistance below the contacts is the same as the sheet resistance of the bare semiconductor film. This assumption seems reasonable since the contacts were not annealed. After extracting the transfer length and the sheet resistance R_{sh} from the plot, the ρ_c value was calculated from the defining relationship:

$$\rho_c = R_{sh} \,.\, L_T^{\,2}. \tag{4}$$

Table I summarizes the R_{sh} and ρ_c values for all of the contacts along with the metal work functions. The R_{sh} values obtained from the analyses described above have been multiplied by the film thickness to give sheet resistivity in Ω cm. The values of the sheet resistivity remained fairly constant for each film type, as expected. One may note that the sheet resistivity for the undoped NCD film is only slightly greater than that for the lightly S-doped film. This small difference is attributed to the reduced mobility in the S-doped films (Table II). The low mobility of all of the films (relative to homoepitaxial films) is attributed to the nanocrystalline structure.

The Schottky barrier height (Φ_B) plays an important role in determining the ρ_c. According to the Schottky–Mott theory, an *n*-type semiconductor Φ_B at the metal-semiconductor interface is determined by the following relationship:[32]

$$\Phi_B = \Phi_M - \chi_S, \tag{5}$$

where χ_S is the electron affinity of the semiconductor. Thermionic and field emission current transport mechanisms indicate that ρ_c exponentially varies with Φ_B.[33] From Table I, the ρ_c values increase with the metal work function for both undoped and S-doped films, suggesting the undoped and S-doped NCD films are *n*-type. Note also that the ρ_c values for the S-doped films were approximately two orders of magnitude lower than those for the undoped films.

TABLE II. Hall-effect measurement results for undoped and S-doped films.

Hall property	Undoped NCD	Doped NCD
Majority carrier type	Electrons	Electrons
Charge density (cm^{-3})	3.5×10^{18}	4.9×10^{19}
Hall mobility (cm^2/V s)	1.2	0.8
Sheet resistivity (Ω cm)	1.5×10^{-1}	1.4×10^{-1}

Table II lists the results from Hall-effect measurements of an undoped and a S-doped film. The values of the sheet resistivity obtained from Hall-effect experiments are in close agreement with those obtained from contact measurements. The sign of the Hall coefficient, which determines the majority carrier type, was found to be negative for both types of films. This result agrees with a recent report on the electrochemical activity of S-doped NCD films, indicating that they are *n*-type.[34] The low carrier mobilities and high charge densities measured in this study are consistent with the nanocrystalline structure of the films. In several disordered semiconductors, such as amorphous Si and Ge, it has been reported that a large excess of charge carriers are required to obtain reasonable modulation of conductivity.[35] In general, the values of the charge densities and carrier mobilities are in agreement with those reported in earlier studies.[36] Theoretical calculations[14,16] and experimental studies[17] on S-doped homoepitaxial diamond films ($N_D \sim 10^{16}$ cm^{-3}) have shown that a small percentage of sulfur $\sim$0.1% is electrically active at ambient temperature. Using the field emission and dc conductivity measurements, Gupta *et al.* proposed that incorporation of sulfur leads to (a) structural defects that result in localized midgap states, (b) increased connectivity of sp^2-bonded grain boundaries which enhanced film conductivity, and (c) a small fraction of sulfur atoms that are electrically active.[37]

B. Photoelectrical measurements

In XPS, the kinetic energy (E_K) of a photoemitted electron is related to its binding energy (E_B), the excitation (photon) energy $h\upsilon$, and the spectrometer work function (Φ) by the following relationship:

$$E_K = h\upsilon - E_B - \Phi. \tag{6}$$

Shifts in the binding energies of the substrate core level peaks after deposition of a thin (<20 Å) metal film were used to measure changes in band bending, from which the Schottky barrier height was determined.

In UPS analysis, the kinetic energy of the emitted electrons bears the same relationship with the spectrometer work function and binding energy as in Eq. (6). The UPS spectra

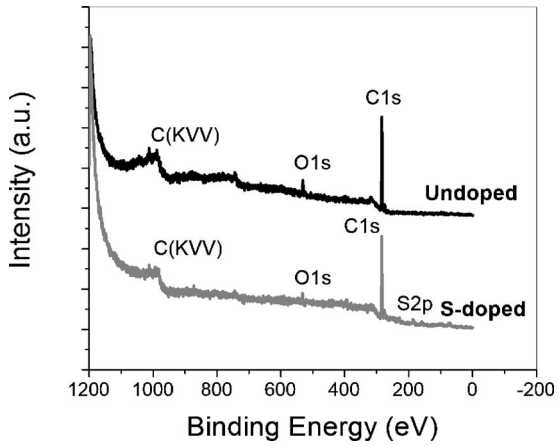

FIG. 3. XPS survey spectra for bare undoped and S-doped NCD films after surface treatment.

were collected to obtain the profile of valence band electronic states, and the position of the Fermi level with respect to the valence band maximum was ascertained.

Figure 3 shows an XPS survey spectra obtained from undoped and S-doped NCD films. From the peak assignments, it is clear that there is oxygen present at the surface despite the annealing and hydrogen plasma treatment. The S $2p$ peak at 164.54 eV binding energy was used for quantitative analysis. Assuming a constant average concentration of S through the bulk of the S-doped NCD film, the atomic concentration of S was estimated to be 0.31%. Experimental studies of homoepitaxial growth on (100) surfaces have indicated that the S concentration saturates at $\sim 10^{16}-10^{17}$ cm^{-3}.[17,18] At higher S concentrations, the crystalline quality of the film degrades suggesting that S may be preferentially incorporated at the grain boundaries. The high concentrations indicated at the surface of the films studied here also suggests that accumulation at the grain boundary is probable. However, experimental studies using techniques such as transmission electron microscopy and secondary-ion mass spectroscopy to probe the bonding environment of sulfur atoms in NCD films would be necessary to confirm the relative concentrations of sulfur in the diamond grains and grain boundaries and its effect on electronic properties.

Figure 4 shows the UPS spectra collected for the bare undoped and S-doped NCD films. The presence of a NEA is evidenced in the UPS spectrum of the undoped film; the sharp peak at low kinetic energy is attributed to secondary electrons that thermalize to the conduction band minimum.[38] The most energetic electrons escape from the surface of the semiconductor. Secondary electrons and electrons that are scattered to lower energies are emitted at lower kinetic energies. It is noted that the UPS spectra cannot be used to determine the value of the electron affinity for a surface which exhibits a NEA.[38]

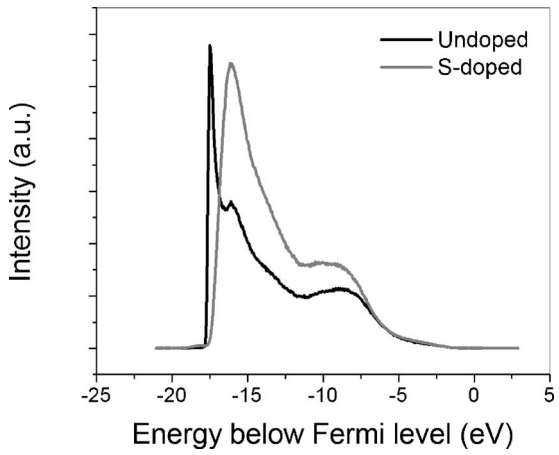

FIG. 4. UPS spectra for bare undoped and S-doped NCD films.

The UPS spectrum of the S-doped NCD film does not indicate the characteristics of a NEA, despite the same surface and cleaning treatment as the undoped film. It is possible that sulfur alters the surface dipole to increase the electron affinity. However, this reasoning is merely speculative and further experimental evidence is needed to understand the effect of doping on the surface properties of NCD films.

In photoelectric studies of diamond (100) and (111) surfaces, a correlation between NEA ($\chi_S \approx 0$) and hydrogen surface termination has been shown.[9] For a material with a NEA,

$$h\upsilon = E_g + W, \tag{7}$$

where $h\upsilon$ (=21.2 eV) is the energy of the incident photons in the UPS measurement, E_g is the band gap of the material, and W is the width of the UPS spectrum. The width of the spectrum shown in Fig. 4 was determined to be 16.2 ± 0.4 eV; it follows that the band gap for the undoped NCD film is 5.0 ± 0.4 eV.

Interestingly, the NEA property is normally associated with sp^3-bonded carbon; however, the 5.0 ± 0.4 eV band gap value is lower than the band gap associated with sp^3-bonded crystalline diamond (5.5 eV). The NCD represents a heterogeneous material consisting of sp^3- and sp^2-bonded carbon. Therefore, we conclude that the band gap calculated in this study is the pseudogap, associated with defect and sp^2-states arising from the grain boundaries that lead to "broadening" of the valence band. The width of the UPS spectrum cannot be accurately ascertained due to this broadening effect and results in uncertainties in the estimation of the pseudogap. The band gap value calculated from photoelectrical measurements in this study is somewhat higher than what is reported for hot-filament CVD grown NCD films from tunneling experiments.[19] Since the S-doped film does not exhibit the NEA property and the electron affinity of the surface is not known, the band gap of the S-doped material could not be calculated.

For n-type semiconductors, the value of E_g is required in the determination of Φ_B from the UPS measurements. Upon close examination of the UPS spectrum for undoped and S-doped NCD films, the position of the Fermi level relative to the valence band edge is determined to be 1.3 ± 0.4 and 1.6 ± 0.2 eV, respectively, indicating that the surfaces are p-type but less so in the S-doped film. This result will be discussed in more detail later.

Figure 5 shows the XPS high resolution C1s spectra for undoped films after successive Ti depositions. A Shirley background was systematically substracted and a mixed Gaussian-Lorentzian line shape was used to fit the C1s spec-

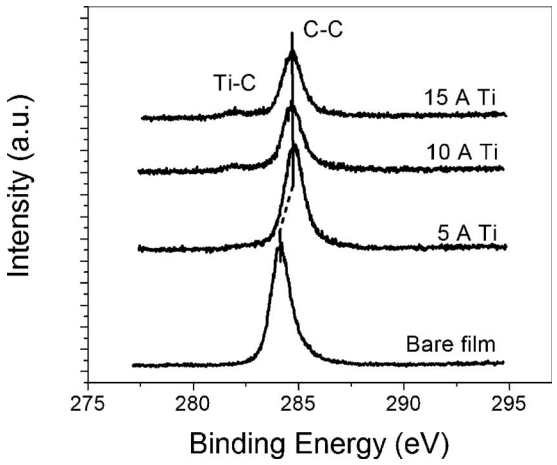

FIG. 5. High resolution C1*s* spectra for an undoped film before and after sequential Ti depositions.

tra. The C1*s* core-level peak moved to a higher binding energy; a peak shift of 0.52 eV was observed after the first 5 Å of Ti deposition. The core-level peak position did not appreciably change after additional depositions of the metal.

Figure 6 shows the UPS spectra of the valance band edge after successive Ti depositions. The sharp increase in the signal at the Fermi level (E_F=0 eV E_B) confirms the metallic nature of the deposited Ti film. Additionally, the O1*s* and C1*s* peak areas decreased with increasing Ti 2*p* peak areas, which occurred with successive metal depositions; this result indicates an increase in metal coverage on the NCD film. Similar spectra have been collected for all the metals on undoped and S-doped films. The Ti metal studies are chosen for illustration.

A deconvolution routine was applied to C1*s* core levels to separate the peak shifts due to the band bending and chemical bonding. Figure 7 shows the high resolution C1*s* spectra for the NCD films with 15 Å layers of Zr and Ti. The small peaks at 281.9 eV and 282.8 eV were attributed to TiC and ZrC, respectively.[39,40] The C-bound-to-C part of the C1*s* spectra was used to calculate the shifts due to band bending.

The UPS analyses of the films suggest that the surface is *p*-type. However, the ρ_c and Hall-effect measurements suggest the films to be *n*-type. Koeck *et al.*[41] have pointed out that the bands bend upward at the surface for the NCD films. Based on the collection of these results, we believe that the bulk of the films are *n*-type and that the surface is inverted (i.e., the surface is *p*-type). Figure 8(a) shows a schematic of the proposed band diagram for the NCD films showing the C1*s* core level.

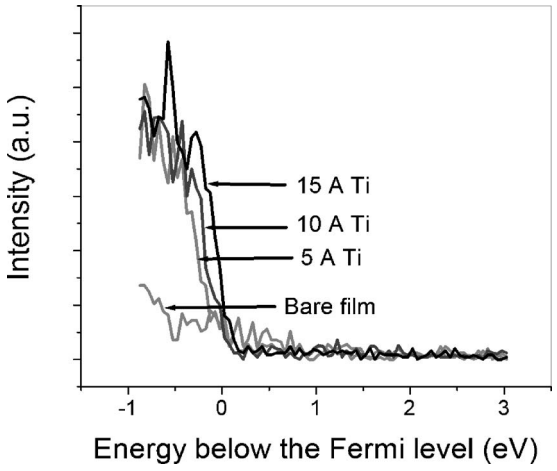

FIG. 6. Valance-band edge from UPS characterization of an undoped NCD film before and after sequential Ti depositions.

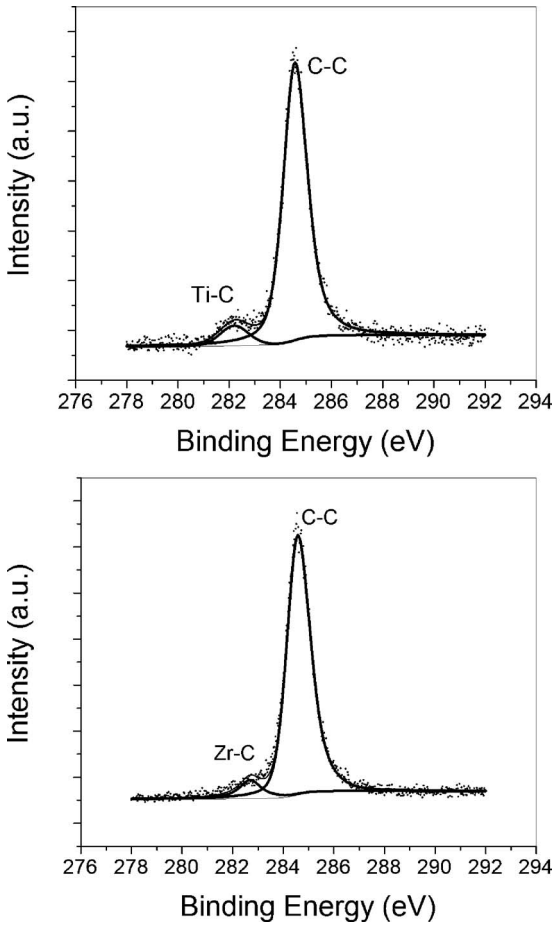

FIG. 7. High resolution C1*s* spectrum for undoped NCD film with 15 Å Ti (top) and 15 Å Zr (bottom) layer showing titanium carbide and zirconium carbide peaks.

The Schottky barrier height has been calculated for each metal-semiconductor interface using the following relationship:

$$\Phi_B = E_g - (E_F - E_V) + (E_{C1s} - E_{C1s}{}^M), \tag{8}$$

where $E_{C1s}-E_{C1s}{}^M$ is the difference in the position of the core level before and after successive metal depositions, and E_F-E_v is the Fermi level position relative to the valence band maximum for a clean semiconductor surface. Figures 8(b)–8(d) show schematics of the energy band diagrams for undoped NCD films after Zr, Ti, and Pt deposition and the corresponding Φ_B values, respectively. For the calculation of Φ_B values, the S-doped films were assumed to have the same band gap as the undoped films, i.e., 5.0 ± 0.4 eV, although Gupta *et al.*[19] reported a modest decrease in the band gap for sulfur concentrations similar to those reported in this study. Hence the values calculated in the present study represent an upper bound for Φ_B for lightly S-doped films. Table III lists

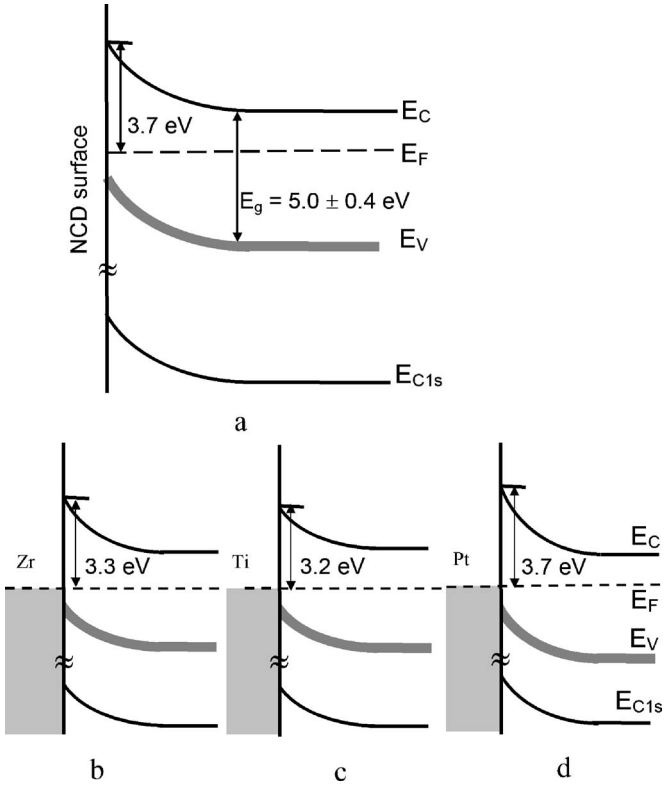

FIG. 8. Schematic of the proposed band diagram for undoped NCD showing band gap (E_g), Fermi level (E_F), conduction band minimum (E_C), valence band maximum (E_V), and C1*s* core-level (E_{C1s}) energies before (a) and after [(b)–(d)] Zr, Ti, and Pt deposition.

the calculated Φ_B values for metals on both the undoped and the S-doped NCD films.

Equation (5) predicts that for a semiconductor with a NEA ($\chi_S \approx 0$ or slightly negative) the Φ_B at the metal-semiconductor interface should be equal to or greater than the metal work function. However, Eq. (5) assumes a flat-band condition at the semiconductor surface prior to metal deposition. In the present case, the surface is depleted (i.e., strong upward band bending) and the surface exhibits a NEA property. From the determinations based on UPS measurements, there is a 3.7 eV barrier from the surface Fermi level to the conduction band minimum, which indicates the presence of surface states in the band gap. Correspondingly, analysis of the XPS core-level peaks indicates partial pinning of the Fermi level; for a 1.6 eV change in the electron work functions of the metals deposited on the undoped NCD films, the calculated Φ_B values change only by 0.4 eV.

Although the Φ_B values at the metal-film interfaces are significantly high, the ρ_c values are very low. A possible reason for this apparent discrepancy could be that the depletion layer is thin enough to permit significant tunneling through the barrier resulting in low ρ_c values calculated from *I-V* measurements. Based on the carrier concentrations from the Hall-effect measurements and the surface barrier from the photoelectrical data, the depletion width was calculated to be 26 nm for undoped NCD. The depletion width and the surface barrier are, therefore, too large for tunneling to account for the low ρ_c values. Considering that variable range hopping is the dominant current mechanism in NCD films,[26] another possibility is that the current passes through localized regions associated with the grain boundaries, whereas the Φ_B calculated from photoelectrical measurements are representative of the large area on NCD diamond. In this case, the grain boundaries (Ohmic regions) would have a much smaller Φ_B than the diamond grains. The *I-V* characteristics and hence the ρ_c would be dominated by the low barrier grain boundary regions while the photoemission measurements and hence the Φ_B would be dominated by the larger area diamond regions. Recent reports on nitrogen-doped (*n*-type) ultra-NCD films attribute the difference in Φ_B values calculated from *I-V* (low) and capacitance-voltage (high) measurements to the heterogeneous mixture of low barrier grain boundary regions and high barrier diamond grains.[42]

TABLE III. Calculated Φ_B at various metal-NCD film interfaces.

Metal	Metal work function Φ_M (eV)	Undoped film Φ_B (eV)	Doped film[a] Φ_B (eV)
Zr	4.05	3.3 ± 0.1	3.0 ± 0.1
Ti	4.33	3.2 ± 0.1	3.1 ± 0.1
Pt	5.65	3.7 ± 0.1	3.4 ± 0.1

[a]Φ_B values for the doped film are based on the assumption that its band gap is same as that of the undoped NCD film.

IV. CONCLUSIONS

Ohmic contacts having low contact resistances in the as-deposited state were fabricated on undoped and lightly S-doped NCD films using four metals (Pt, Cu, Ti, and Zr) that span a wide range of electron work functions. The ρ_c values increased with metal work function and decreased with S-doping. The combination of the *I-V* data, the Hall data, and the photoemission analyses led to the conclusion that the films are *n*-type with inverted *p*-type surfaces. Furthermore, the UPS characterization showed that the undoped NCD films have a NEA. The NEA property of the undoped NCD films permitted estimation of the pseudo gap for the material (5.0 ± 0.4 eV). Based on the results from the present study and with reference to earlier studies, an electron band structure model was proposed. Schottky barrier heights of each metal on undoped and S-doped NCD films were calculated based on *in situ* XPS core-level analysis and the proposed electron band model. The Schottky barrier heights were found to increase with metal work function, corroborating the results obtained from electrical measurements. With the potential for reliable, low-resistance Ohmic contacts, a variety of electronic devices based on NCD films are possible.

ACKNOWLEDGMENTS

The authors gratefully acknowledge support from the National Science Foundation (Grant Nos. DMR-0304508 and DMR-0354939) and from the ONR MURI on Thermionic Energy Conversion (Program Manager Mihal Gross). Appreciation is also expressed to Dr. M. C. Zeman and Joshua R. Smith of North Carolina State University for the evaporation of metal films for the photoelectric characteriza-

tions. Some of the films in this study were grown using equipment funded the National Science Foundation (Grant No. DMR-9802917).

[1]R. J. J. Rioboo and M. Belmahi, J. Appl. Phys. **97**, 073509 (2005).
[2]H. J. Looi, L. Y. S. Pang, Y. Wang, M. D. Whitfield, and R. B. Jackman, Diamond Relat. Mater. **7**, 565 (1998).
[3]T. Sharda, M. M. Rahaman, Y. Nukaya, T. Soga, T. Jimbo, and M. Umeno, Diamond Relat. Mater. **10**, 561 (2001).
[4]W. Yang, O. Auciello, J. E. Butler, W. Cai, J. A. Carlisle, J. Gerbi, D. M. Gruen, T. Knickerbocker, T. L. Lasseter, J. N. Russell, L. M. Smith, and R. J. Hamers, Nat. Mater. **2**, 63 (2003).
[5]A. R. Krauss, O. Auciello, D. M. Gruen, A. Jayatissa, A. Sumant, J. Tucek, D. C. Mancini, N. Moldovan, A. Erdemir, D. Ersoy, M. N. Gardos, H. G. Busmann, E. M. Mayer, and M. Q. Ding, Diamond Relat. Mater. **10**, 1952 (2001).
[6]H. Taniuchi, H. Umezawa, T. Arima, M. Tachiki, and H. Kawarada, IEEE Electron Device Lett. **22**, 390 (2001).
[7]J. E. Yater, A. Shih, J. E. Butler, and P. E. Pehrsson, J. Appl. Phys. **96**, 446 (2004).
[8]F. J. Himpsel, J. A. Knapp, J. A. Van Vechten, and D. E. Eastman, Phys. Rev. B **20**, 624 (1979).
[9]J. van der Weide, Z. Zhang, P. K. Baumann, M. G. Wensell, J. Bernholc, and R. J. Nemanich, Phys. Rev. B **50**, 5803 (1994).
[10]M. Nesladek, Semicond. Sci. Technol. **20**, R19 (2005).
[11]P. Achatz, J. A. Garrido, M. Stutzmann, O. A. Williams, D. M. Gruen, A. Kromka, and D. Steinmuller, Appl. Phys. Lett. **88**, 101908 (2003).
[12]R. Kalish, Carbon **37**, 781 (1999).
[13]S. Koizumi, M. Kamo, Y. Sato, H. Ozaki, and T. Inuzuka, Appl. Phys. Lett. **71**, 1065 (1997).
[14]D. Saada, J. Adler, and R. Kalish, Appl. Phys. Lett. **77**, 878 (2000) and references therein.
[15]M. Kubo, A. Miyamoto, M. N. Gamo, and T. Ando, Jpn. J. Appl. Phys., Part 1 **40**, 2830 (2001).
[16]Y. Cai, T. Zhang, A. B. Anderson, J. C. Angus, L. N. Kostadinov, and T. V. Albu, Diamond Relat. Mater. **15**, 1868 (2006).
[17]I. Sakaguchi, M. N. Gamo, Y. Kikuchi, E. Yasu, H. Haneda, T. Suzuki, and T. Ando, Phys. Rev. B **60**, R2139 (1999).
[18]M. N. Gamo, C. Xiao, Y. Zhang, E. Yasu, Y. Kikuchi, I. Sakaguchi, T. Suzuki, Y. Sato, and T. Ando, Thin Solid Films **382**, 113 (2001).
[19]S. Gupta, B. R. Weiner, and G. Morell, J. Appl. Phys. **97**, 094307 (2005).
[20]S. Gupta, A. Martinez, B. R. Weiner, and G. Morell, Appl. Phys. Lett. **80**, 1471 (2002).
[21]S. Bhattacharyya, K. Walzer, H. Hietschold, and F. Richter, J. Appl. Phys. **89**, 1619 (2001).
[22]C. Brosseau, F. Boulic, P. Queffelec, C. Bourbigot, Y. Le Mest, J. Loaec, and A. Beroual, J. Appl. Phys. **81**, 882 (1997) and references therein.
[23]P. Achatz, J. A. Garrido, M. Stutzmann, O. A. Williams, D. M. Gruen, A. Kromka, and D. Steinmuller, Appl. Phys. Lett. **88**, 101908 (2006).
[24]J. Robertson and E. P. O'Reilly, Phys. Rev. B **35**, 2946 (1987).
[25]G. Fanchini, S. C. Ray, and A. Tagaliaferro, Diamond Relat. Mater. **12**, 891 (2003).
[26]J. van der Weide, Ph.D. thesis, North Carolina State University, 1994.
[27]D. K. Schroeder, *Semiconductor Material and Device Characterization* (Wiley, New York, 1998).
[28]G. K. Reeves and H. B. Harrison, IEEE Electron Device Lett. **3**, 111 (1982).
[29]G. S. Marlow and M. B. Das, Solid-State Electron. **25**, 91 (1982).
[30]B. Jacobs, M. C. J. C. M. Kramer, E. J. Geluk, and F. Karouta, J. Cryst. Growth **214**, 15 (2002).
[31]M. C. J. C. M. Kramer, M.Sc. thesis, Technical University of Eindhoven, 2000.
[32]E. H. Rhoderick and R. H. Williams, *Metal Semiconductor Contacts*, 2nd ed. (Oxford University Press, Oxford, 1988), p. 12.
[33]S. M. Sze, *Physics of Semiconductor Devices*, 2nd ed. (Wiley-Interscience, New York, 1999), pp. 262, 304.
[34]I. Gonzalez-Gonzalez, J. De Jesus, D. A. Tryk, G. Morell, and C. R. Cabrera, Diamond Relat. Mater. **15**, 221 (2006).
[35]N. F. Mott and E. A. Davis, *Electronic Processes in Non-Crystalline Materials* (Clarendon, Oxford, 1971), pp. 37, 198.
[36]G. Morell, A. Gonzalez-Berrios, B. R. Weiner, and S. Gupta, J. Mater. Sci.: Mater. Electron. **17**, 443 (2006).
[37]S. Gupta, G. Morell, and B. R. Weiner, J. Appl. Phys. **95**, 8314 (2004).
[38]R. J. Nemanich, P. K. Baumann, M. C. Benjamin, J. Van der Weide, S. W. King, and R. F. Davis, Diamond Relat. Mater. **5**, 790 (1996).
[39]H. Ihara, Y. Kumashiro, A. Itoh, and K. Maeda, Jpn. J. Appl. Phys. **12**, 1462 (1973).
[40]R. Kaufmann, H. Klewe-Nebenius, H. Moers, G. Pfennig, H. Jennet, and H. J. Ache, Surf. Interface Anal. **11**, 502 (1988).
[41]F. A. M. Koeck, J. M. Garguilo, R. J. Nemanich, S. Gupta, B. R. Weiner, and G. Morell, Diamond Relat. Mater. **12**, 474 (2003).
[42]T. Zimmermann, M. Kubovic, A. Denisenko, K. Janischowsky, O. A. Williams, D. M. Gruen, and E. Kohn, Diamond Relat. Mater. **14**, 416 (2005).